Gene network architecture, mutation and selection collectively drive developmental pattern evolvability and predictability

Harry Booth[1] and Z. Hadjivasiliou[1,2,3]

[1] *The Francis Crick Institute: Mathematical and Physical Biology Laboratory, 1 Midland Road, London, NW1 1AT, UK*

[2] *University College London: Department of Physics and Astronomy, Gower Street, London, WC1E 6BT, UK*

[3] *London Centre for Nanotechnology, 19 Gordon Street, London, WC1H 0AH, UK*

November 16, 2024

Abstract

Much of the striking diversity of life on earth arises from mutations in conserved regulatory elements that govern reduced modules of Gene Regulatory Networks (GRNs). Although the mechanistic basis by which GRNs orchestrate cellular responses and tissue patterning during development is well understood, their evolutionary dynamics remain less clear. In this study, we probe how key evolutionary forces such as mutation, selection and historical contingency interact with GRN architecture to drive the diversification of developmental mechanisms and patterns. We introduce a novel high-throughput theoretical framework for GRN-driven pattern evolution to produce a comprehensive dataset of evolutionary trajectories. Utilizing computational and machine learning methods, we interpret this data within an evolutionary context. Our results elucidate the interplay between mutational and ecological influences and network architecture, revealing how historical contingencies affect the evolvability of GRNs and the predictability of their evolutionary outcomes. This work echoes recent synthetic and laboratory evolution experiments as well as comparative studies, providing a mechanistic basis for their interpretation. Our framework offers a powerful and adaptable platform for the investigation of GRN-drive pattern evolution, that links physical constraints that emerge from genetic architecture to evolutionary change and diversification.

Introduction

A central challenge in evolutionary developmental biology is to elucidate how phenotypic variation arises from underlying developmental mechanisms. At the core of development lies the spatial patterning of tissues into different cell types, driven by gene regulatory networks (GRNs) that interpret morphogen gradients[1]. While the mechanistic basis of how GRNs influence spatial patterning during development is well-established, the interplay of these networks with evolutionary forces such as mutation, selection, and historical contingency remains poorly understood. Yet, several studies have revealed the critical role of GRNs in generating morphological variation both within and across species[2–6], underscoring the importance of investigating their evolutionary dynamics in this developmental context.

Recent experimental efforts are narrowing this gap in our understanding. For instance, studies leveraging synthetic networks have begun to place patterning GRNs in an evolutionary context by constructing "neutral networks" – GRNs connected by small mutational changes that produce the same phenotype – to explore how evolution navigates the genotype landscape and generates novel phenotypes through non-adaptive processes[7]. Additionally, mutational assays in synthetic systems have quantified epistasis within patterning GRNs[8] while also probing how network architecture determines phenotypic accessibility and evolvability[9]. Complementary *in vivo* mutagenic studies in model organisms such as *Drosophila* have provided insights into the relationship between the type and magnitude of mutations on regulatory elements and their impact on pattern formation during embryonic segmentation[10]. Furthermore, enhanced capabilities for parallel laboratory evolution experiments in fruit flies are beginning to shed light on the role and predictability of GRNs under stabilizing selection for development patterns[11]. Together these investigations raise a crucial question: how do these phenomena emerge and shape evolutionary trajectories as new developmental patterns emerge and diversify? The complexity of GRN-driven patterning, characterized by multi-scale, multi-component, and nonlinear dynamics, coupled with the timescales over which evolutionary change occurs, present challenges that experimental tools alone may struggle to overcome.

Theoretical models of GRN-driven patterning have successfully captured the spatiotem-

poral patterning dynamics observed in various model systems, from the *Drosophila* embryo[12–14] to the vertebrate neural tube[15,16]. While these models do not explicitly track genetic information at a molecular scale, they have provided crucial mechanistic insights into the fundamental characteristics and emergent properties of GRN patterning[17–19], and offer a promising and tractable framework for exploring GRN-driven pattern evolution. Previous work integrating mechanistic GRN patterning models into evolutionary simulations has yielded valuable insights into the constraints and design principles that optimize specific phenotypic outcomes, or "fitness"[20–22]. For example, simulations have identified parsimonious paths in GRN space linking Dipteran species and their homologous relationships[23], elucidated the design principles underlying body plan segmentation in flies[24], and explored potential routes toward the *de novo* evolution of body segmentation[25,26]. This mechanism-centered approach highlights the central role of gene interactions and network topology – rather than individual genes – as key drivers of evolutionary processes.

In this work we explore the interplay between mutational processes, network architecture, and natural selection in shaping the evolution of GRNs and developmental patterns, as well as the predictability of evolutionary dynamics. We present a high-throughput and generalizable theoretical framework that integrates a mechanistic model of GRN patterning with ecological and evolutionary parameters. By leveraging the framework's capacity for large-scale data generation, we produce an extensive dataset of evolutionary trajectories. We then employ computational and machine learning techniques to extract general principles of GRN-driven pattern evolution and provide mechanistic insights into recent experimental observations. Our analysis distinguishes between mutations that establish *de novo* gene boundaries and those that refine existing boundaries, while also elucidating how the strength of selection and genetic drift influence the evolution of patterns and GRN architecture. Moreover, we exploit the scale of the data generated to build a predictive framework of GRN pattern evolution. By bridging the classic concept of evolutionary contingency with modern machine learning techniques, we develop a probabilistic framework for investigating how historical mutations can shape the evolutionary trajectory of GRNs and developmental patterns. This approach revisits the long-standing debate between contingency and necessity in evolutionary biology, originally posed by Stephen Jay Gould[27], now contextualized within the fundamental developmental process of GRN-mediated pat-

terning.

In summary, this work provides universal insights into the evolution of GRN-mediated patterning and establishes a versatile and powerful framework that links the physical constraints that emerge from genetic architecture to evolutionary change. In this way, the findings of our work and future applications of the tools we have developed can be used to interpret both recent and future laboratory and synthetic evolution experiments as well as comparative studies, and bridge the gap between physics, mechanistic constraints of dynamical systems and evolutionary theory.

Results

A high-throughput framework for GRN evolution

We model the *de novo* evolution of a stripe in a GRN patterning system through mutation of the regulatory interactions between genes. Our theoretical framework encompasses three key components (fig. 1): i) GRN-mediated spatial patterning, ii) mutation and fitness evaluation, and iii) a Monte-Carlo scheme which simulates an evolutionary trajectory.

We consider a 1-dimensional tissue composed of a discrete number of cells, over which a morphogen gradient is established (fig. 1.A). Each cell has an identical GRN consisting of 3 genes $\{a, b, c\}$, with gene a activated by the morphogen, m (fig. 1.A-B). The network is specified by a weight matrix W whose entries w_{ij} encode the pairwise regulatory interactions between genes (fig. 1.B). The evolutionary starting point in our simulations is given by an initial weight matrix, W_0, with a minimal number of non-zero interactions (fig. 1.C), representing an initial constraint. New GRN functionalities are thought to evolve through the re-use of existing regulatory components[28–31] between which novel interactions evolve, producing a specialised function[32]. Hence, subsequent mutation and selection is expected to drive the addition of new regulatory interactions between genes to generate novel patterns.

The level of abstraction at which the genotype is represented determines what features of mutation can be captured in a computational implementation of evolution and in what detail[33,34]. The weight matrix W represents the genotype in our model, and mutation acts

directly on its entries to produce a mutant GRN. Previous work has suggested that multiplicative weight changes most accurately represent the effect of point mutations on binding affinities in transcription factor (TF) binding sites[35]. We model this as $w_{ij}^{n+1} = w_{ij}^{n} \exp(k)$, where k is normally distributed with $k \sim N(\mu_M, \sigma_M^2)$ and w_{ij}^{n} and w_{ij}^{n+1} represent the regulatory effect of gene i on j before and after mutation respectively. Typically point mutations in binding sites decrease affinity[35,36], and so we set $\mu_M < 0$. Point mutations can generate *de novo* regulatory interactions[37], but changes of larger effect may occur though mechanisms such as duplication[32,38] or co-option[6,39]. Therefore, we also consider additive weight changes such that $w_{ij}^{n+1} = w_{ij}^{n} + k$, where k is normally distributed with $k \sim N(0, \sigma_A^2)$. This allows the distribution of weight change magnitudes $|w_{ij}^{n+1} - w_{ij}^{n}|$ to be independent of the initial magnitude $|w_{ij}^{n}|$ and enables the sign of the interaction to change from activating to inhibiting or vice versa. A single mutant may carry multiple weight changes simultaneously. Each weight in W is mutated independently with probability p, reflecting an effective mutation rate. Multiple weight changes can occur through various mechanisms, for example when mutations on the same enhancer affect the binding affinity of multiple TFs, or when TFs themselves mutate. Multiple simultaneous weight changes therefore encapsulate a higher-order level of network re-organization through changes at the sequence level[39–41].

We investigate the evolution of novel gene expression boundaries, by implementing selection for a stripe pattern. The formation and adjustment of gene expression boundaries is a hallmark of developmental patterning and its evolution and so this approach has the potential to yield general insights about the evolution of development. We define a target stripe by a specific width and position (fig. 1.A), and compute the fitness differential $\Delta\mathcal{F}$ of mutants relative to the resident phenotype (fig. 1.C). We assume that selection acts on the steady state expression profile of gene c and model monomorphic evolutionary dynamics with a sequential fixation model, by assuming that the mutation rate is lower than the time it takes for mutants to fix[42,43]. The Monte-Carlo scheme for an evolutionary trajectory is defined by the probability that a mutant fixes in a population of size P_s:

$$p = \frac{1 - \exp\left(-2\beta\Delta\mathcal{F}\right))}{1 - \exp\left(-2P_s\beta\Delta\mathcal{F}\right)} \tag{1}$$

where β represents the strength of selection[44].

We use this theoretical framework to simulate a large number ($\sim 10^5$) of evolutionary trajectories from the initial genotype W_0 to a final stripe-producing genotype W_N. We use this data to address *how* the genotype interacts with mutation and ecological parameters, to drive phenotypic variation and the emergence of novel functionalities.

Refer to SM for further details on the dynamical equations, evolutionary algorithm and parameters used.

Multiple GRN topologies evolve following selection for stripe phenotype

We start by characterising the network topologies that evolved across our simulations. To do this, we recorded the evolutionary trajectory $(W_n^{(i)})_{n=0}^{N_i}$ of accepted genotypes, where N_i is the total number of accepted mutants required to reach the target phenotype for the ith trajectory (fig. 1.C). Across evolutionary trajectories we defined four key stages; the first accepted mutant ($n = 1$), a period of pre-stripe formation for $n \in (1, S_0)$, stripe inception ($n = S_0$) and post-stripe formation for $n \in (S_0, N_i]$. Therefore, S_0 is the mutant number for which a stripe first manifests (fig. 2.A). To characterise the mechanistic outcomes of individual trajectories, we identified the minimal subset of regulatory interactions that maintain a basic stripe phenotype, or *minimal stripe topology (MST)*, for the evolved networks at $n = S_0$ and $n = N_i$, denoted $M_{S_0}^{(i)}$ and $M_{N_i}^{(i)}$ respectively (fig. 1.C and SM). This is similar in spirit to fitness-based network reduction[45] and the "essential network"[46], aiming to identify the core stripe-forming dynamics[47].

Using this information we infer a distribution of unique evolutionary outcomes relating to the core mechanisms of stripe formation (fig. 2.B). We identified a total of 732 unique MSTs, with the eight most frequent (MST:1-8) accounting for $\sim$75% of outcomes. The remaining MST outcomes occurred with a frequency $\leq 1.62\%$. MST:$\{1, 2, 5, 6, 7\}$ feature the well-studied feed-forward incoherent type-2 (I2-FFL) mechanism, found in the gap gene network responsible for embryo segmentation in fruitflies[47,48]. MST:4 is the I3-FFL mechanism[49], which has not been observed in natural stripe-forming regulatory networks but has been investigated synthetically[9]. MST:$\{3, 8\}$ feature a negative feedback loop with

gene B serving as a controller to determine different responses across inputs, a mechanism which has been shown to enable perfect biochemical adaption[50].

Following (Cotterell and Sharpe, 2010), we solve each of the network dynamics to steady state and collect concentration profiles at intermediary times[47] (see SM). A 2D projection of these high dimensional dynamical profiles confirms that each of the top 4 MSTs represents a broadly distinct dynamical mechanism (fig. 2.C). MST:2 and MST:3 are topologically contained in MST:6 and MST:8 respectively, which translates to dynamical similarity in the projection. By contrast, MST:2 also contains MST:1 but presents distinguishable dynamics. This highlights that topological measures of similarity such as Hamming distance or strict inclusion are not always consistent with dynamical similarity.

In the example trajectory shown in Figure 2.A, the MST associated with the initial and final stripe forming networks are the same ($M_{S_0} = M_N$). Therefore, after the key phenotypic transition to a stripe has been achieved, refinement of the boundaries occurred without additional mechanistic innovation. We found that this was often true across our simulations (fig. 2.D). Analogously, embryonic patterning typically involves deeply conserved networks, with species specific variations likely achieved through adjustment of interaction strengths[5,51,52].

We identified 3 additional scenarios related to mechanism preservation across our simulations (fig. 2.D). In some cases the final mechanism contains additional but necessary interactions whilst maintaining the initial MST interactions ($M_{S_0}^{(i)} \subset M_{N_i}^{(i)}$), representing "complexification" of the mechanism. Alternatively, the final mechanism represents a simplification of the original ($M_{N_i}^{(i)} \subset M_{S_0}^{(i)}$), whereby core interactions have been removed without losing the stripe phenotype. Finally in rare cases a fundamental mechanistic shift occurs; at least one core interaction present in both the initial stripe forming network and final network differs in sign ($M_{S_0}^{(i)} \not\subset M_{N_i}^{(i)} \wedge M_{N_i}^{(i)} \not\subset M_{S_0}^{(i)}$).

Whilst rare, this latter scenario echoes observations made in evolution experiments, in which GRNs were selected to have differing responses in a modulating environment[53]. Here, topological innovations were required to overcome conflicting objectives, while changes in regulatory strengths that preserved network topology were sufficient to drive evolution in the absence of conflict. A question that follows is what type of pattern or functional

innovation necessitates mechanistic innovation at the GRN level. The scenarios for which $M_{S_0}^{(i)} \neq M_{N_i}^{(i)}$ suggest that there are conditions in which the mechanism evolved at $n = S_0$ cannot easily produce the necessary boundary adjustment, which requires either the evolution of an increasingly baroque structure or a fundamental re-organization of regulatory mechanism. Therefore the evolvability of a network becomes contingent upon the historical sequence of mutations and the resulting mechanism as suggested before[9,54].

Phenotypic transitions and mutational constraints during stripe evolution

Given the mechanistic variation we observed in the final evolved networks (fig. 2.B), we wondered whether there was similar variation in the phenotypic transitions produced through selection. To answer this we characterised the phenotypic transition associated with each accepted mutant. We reasoned that there are three "routes" to a stripe pattern (fig. 3.A). Starting from the shallow left boundary associated with the initial genotype, evolution can first establish a sharp left boundary followed by a sharp right boundary through sequential mutants, do this in reverse, or establish both left and right boundaries simultaneously (coloured arrows in fig. 3.A). In between establishing new boundaries, mutation and selection can continue to alter the phenotype, e.g. by adjusting the location or amplitude of existing boundaries (self loops in fig. 3.A). Finally, mutants can be phenotypically neutral, creating no observable changes and no fitness change compared to the resident phenotype.

Figure 3.B summarises when these phenotypic transitions are observed across our evolutionary trajectories. We found that 98.8% of trajectories introduced the left boundary first followed by the right boundary. The vast majority (98.4%), establish the left boundary with the first accepted mutant ($n = 1$), followed by adjustment of the newly formed left boundary to align it with that of the target stripe ($1 < n < S_0$). The right boundary is established at $n = S_0$, with its location then similarly adjusted to match the target pattern during $n > S_0$. The prominence of this phenotypic path is consistent with the initial network topology, in which the morphogen inhibits output gene c (orange node) through the intermediary gene a (grey node) (fig. 1.C). This initial constraint means that

creating the left boundary simply requires increasing positive feedback on gene c. Accordingly, $\sim 96\%$ of accepted mutations at $n = 1$ introduce a self-activation interaction on gene c, and altering the initial network configuration impacts the sequence of phenotypic transitions (fig.S1,S2). The wait times associated with the acceptance of mutants in each evolutionary period indicate that the left boundary is typically established quickly (fig. 3.C). In contrast, establishing the right boundary at $n = S_0$ takes orders of magnitude longer. In summary, phenotypic trajectories are highly stereotyped, and reflect the differential phenotypic accessibility of traits imposed by the initial constraint.

To understand how the mutational process interacts with the current genotype and selection to produce phenotype transitions we characterised the types of weight changes carried by mutants accepted within each evolutionary period (fig. 3.D). Mutants accepted in periods $1 < n < S_0$ and $n > S_0$ primarily carry adjustments to existing weights, and weight changes during these periods are typically of smaller magnitude (fig. 3.E). These periods are associated with the movement of existing boundaries, supporting the conclusion that the refinement of existing patterns is primarily achieved through small adjustments to the existing network. In contrast, formation of new boundaries at $n = 1$ and $n = S_0$ typically required the addition of novel regulatory interactions (fig. 3.D) and was often associated with weight changes of larger effect (fig. 3.E). Additionally, right boundary formation was frequently associated with weight sign change (fig. 3.D). Therefore, generating novel gene expression boundaries requires more extensive network re-organization. These findings explain observations made in the fly embryo, whereby point mutations in existing enhancers led to changes in expression levels that were typically restricted to the native pattern, whereas new patterning phenotypes emerged through insertion of novel enhancer elements[10].

Next we characterised the number of weight changes per accepted mutant in each evolutionary period (fig. 3.F). Pre-selection, the mutation rate specifies a null distribution for the number of weight changes per mutant (crosses, fig. 3.F[i] - for derivation see SM). Post-selection this null distribution is "re-balanced", representing the number of weight changes carried by accepted mutants (bars, fig. 3.F[i]). Mutants carrying more weight changes represent a higher *realised* mutation rate. Therefore, this analysis is analogous to investigating correlations between mutation rates and selection coefficients[55]. For $n = 1$

and $n = S_0$ we noted a bias for more weight changes in accepted mutants. The probability that a stripe-forming mutant carries only a single weight change is $\sim 3\%$, compared to the null expectation of $\sim$60% (fig. 3.F[i]). A similar bias, albeit less pronounced, is observed for $n = 1$. Conversely, the number of weight changes carried by mutants in periods $1 < n < S_0$ and $n > S_0$ follow the null distribution.

For each mutant carrying multiple weight changes we additionally evaluated the minimum number of weight changes that were strictly necessary to achieve the observed fitness gain (heat maps in fig. 3.F[i]). This evaluation reveals 1) when multiple weight changes were strictly necessary for the original fitness gain and 2) when weight changes interact with one another to impact the phenotype, demonstrating epistasis. The evaluations shown in Figure 3.F[ii] reveal that many of the initial mutants ($n = 1$) carrying multiple weight changes could achieve the associated fitness gain using only a single weight change. The selective advantage for multiple weight changes at $n = 1$ can be understood in context of the minimality of the network at this stage of evolution. Because few interactions are initially present, new interactions are more likely to have no regulatory effect on the output gene and hence be phenotypically neutral. Introducing more weight changes merely increases the likelihood that a consequential interaction is introduced (fig.S3). This highlights how correlations between mutation rates and selection coefficients can emerge merely from having a finite mutational target size, particularly when only a small number of beneficial mutations are accessible[55].

At $n = S_0$, the increasing number of weight changes carried by accepted mutants is necessary for the associated fitness advantage (fig. 3.F[ii]). To explain the selective bias towards multiple weight changes at $n = S_0$, note that stripe formation in our evolved networks is achieved largely through incoherent feed-forward or negative feedback loops (fig. 2.B). The correct function of these mechanisms involves precise interactions between participating genes[56], thereby requiring coordinated evolutionary changes of multiple weights. Additionally, in many instances of stripe evolution we found that the regulatory pathway $a \rightarrow b \rightarrow c$ (fig. 1.B) must be created *de novo* to form a variant of feed-forward loop (fig.S4). Yet, the change in phenotype resulting from the addition of $a \rightarrow b$ is neutral unless $b \rightarrow c$ is also present. This is an example of adaptation involving neutral intermediate mutations of a multi-interaction trait[57], since any one of the required weight changes is often neutral indi-

vidually. To highlight this effect we increased the likelihood of accepting neutral mutants by reducing the effective population size, and restricted the mutational process to generate only single weight changes per mutant. In this high-drift regime mutants could frequently establish a stripe using a single weight change at a time (fig.S5,S6). This demonstrates that correlations between mutation rates and selection coefficients depend on population parameters in network evolution, which has been discussed in the context of molecular evolution previously[55,57,58].

Functional epistasis arises between genes that act within the same regulatory pathway[59], and has been documented in synthetic incoherent feed-forward network motifs by introducing cis-regulatory mutations into multiple genes simultaneously[8,9]. For $n > S_0$ the complete set of weight changes was more frequently required for the fitness gain associated with mutants carrying multiple weight changes, compared to $1 \leq n < S_0$ (fig. 3.F[ii]). We posit that this is due to the non-linearity inherent to incoherent/negative feedback loops[60], and more generally due to the pleitropy arising through increased network "connectedness"[61]. To disentangle the effect of network sparsity in this comparison, we removed the mutants carrying weight changes with no effect on the output gene, which confirmed the higher level of dependency between weights in mutants post-stripe formation compared with earlier periods (fig.S7). In addition, we noted an increased frequency of non-additive fitness effects in $n > S_0$ compared with earlier periods (fig.S8). These observations indicate that the mechanistic innovation required for stripe formation at $n = S_0$ is accompanied with increased epistatic effects in $n > S_0$.

A predictive framework reveals constraints and contingencies of GRN evolution

Given that evolutionary constraints can be imposed by the underlying patterning mechanism[9,54], we wondered to what extent future evolutionary paths become contingent upon the weight changes accepted in intermediate steps. To this end, we built a predictive model of MST outcome given the regulatory interactions present at any point in an evolutionary trajectory. For the purpose of training a probabilistic classifier we limited ourselves to the top 4 MST's (65.4% of trajectories; fig. 2.B), with an additional "Other" category

representing the remaining MST examples (34.6%). Details of the training procedure can be found in SM.

The trained classifier yields probabilities for the different MST outcomes given the current network in an evolutionary trajectory. An example trajectory and its associated predictions is shown in Figure 4.A. This trajectory consisted of four accepted mutants before stripe inception at $n = S_0 = 4$. The initial prediction $p^{(i)}(0)$ simply reflects the proportion of each MST observed in the train-set - the null prediction learnt by the model given the initial constraint. Following the first accepted mutant a new prediction, $p^{(i)}(1)$, indicates that the network changes have increased the likelihood that MST:1 will be adopted at the point of stripe formation. Following the second accepted mutant MST:4 becomes the most likely outcome, and forms a correct prediction which persists until S_0.

We describe a mutant which changes the MST outcome prediction as branching (see SM). Therefore in the above example, the second mutant was branching. These types of mutants are important since they represent the incorporation of regulatory constraints which change the likely path of evolution, and establish a methodological connection with probabilistic characterisations of evolutionary contingency[62]. Figure 4.A shows how the statistical entropy $H(\cdot)$ associated with the predicted probabilities $p^{(i)}(k)$ changes as mutants fix. Interpreting the entropy as a measure of uncertainty inherent to the MST outcome, this example highlights the intuitive notion that uncertainty decreases as evolution progresses (fig.S9A). We found this to be a general principle, with mutants and their corresponding network changes often decreasing uncertainty in eventual MST outcome (fig.S9B), in agreement with the observation that the space of possible evolutionary paths that a trait can take tends to narrow during its evolutionary history[63,64].

We next asked how early in evolution it was typically possible to make correct predictions about the final MST outcome. We found that when networks had accumulated between 45-65% (average in bin: 57%) of their total weight changes at $n = S_0$, the percentage of correct predictions varied between 48% and 65% depending on the MST outcome to be predicted (fig. 4.B[i]). This suggests a higher degree of uncertainty in the evolutionary paths associated with particular MSTs. The predictive performance of the model deteriorated when only topological information was considered by the classifier (fig. 4.B[i] versus

[ii]), indicating that network topology alone is not sufficient for determining the likely path of evolution and that the magnitude of the interactions between genes matter.

We then investigated whether we could steer evolution towards a particular MST outcome by "engineering" the initial mutant. We used the predictive model to identify initial ($n = 1$) mutants that were branching towards a specific MST outcome and identified the branching mutant producing the largest negative entropy change, implying a highly certain mechanistic prediction. To aid tractability, we focused on mutants carrying 2 weight changes relative to the initial network. The mutants found through this procedure for MST:2 and MST:3 both induce the same change in fitness and hence have an equal probability of fixation (fig. 4.C[i]). Interestingly, these mutants induce the same topological change, however differences in the weight values result in alternative mechanistic predictions (fig. 4.C[ii]). We then imposed the identified mutations at $n = 1$ and simulated 5000 independent trajectories from these new initial conditions. In both instances evolution was steered towards the predicted mechanism (fig. 4.C[iii-iv]), while similar results were observed for mutations predicted to steer evolution towards other MSTs (fig.S10). This suggests that regulatory interactions incorporated early in network evolution can significantly bias evolution towards a specific mechanistic outcome, and highlights the important role of historical contingency in GRN evolution[27].

Recall that multiple weight changes were often accepted at $n = 1$, not all of which were strictly necessary. Each adaptive weight change at $n = 1$ therefore likely fixed with a non-adaptive weight change, reminiscent of genetic hitchhiking[65]. Neutral or nearly neutral network changes may provide a reservoir of cryptic genetic variation for subsequent evolution[31], which enables paths to new adaptive genotypes and creates historical contingency in protein evolution[66]. We explore this idea in the context of regulatory evolution by using our predictive model to identify which weight changes carried by a mutant contributes most strongly to its mechanistic prediction. This is achieved by viewing weights as predictive "features" within a game theoretic feature explainability framework[67].

For each weight change we use this framework to produce a prediction attribution, Φ, which encapsulates to what extent an individual weight change shifts the prediction for the MST outcome of evolution (see SM). To then identify the relative importance of the hitchhiking

versus adaptive weight change in relevant mutants we calculate the ratio $\Phi_{\text{carrier}}/\Phi_{\text{hitchhike}}$. In the majority of such accepted mutants, the hitchhiking weight change is far more instrumental in determining the mechanistic outcome than the weight change associated with the carrier (fig. 4.E). This suggests that regulatory networks can accumulate selectively-neutral constraints which significantly alter the likely course of evolution, demonstrating a complex interplay between neutral evolution and historical contingency. This conclusion has also been reached experimentally in a transcription network that controls the response to mating pheromone in yeast[68], where the gain of a neutral regulatory interaction permitted changes in the overlapping circuit responsible for pheromone induction.

Discussion

In this work we have examined how the architecture of developmental mechanisms interacts with evolutionary processes. By placing GRNs in an evolutionary context we have elucidated the complex, multi-layered process through which gene network architecture, mutation and natural selection together determine evolutionary outcomes. The dynamical interplay of these forces in the context of adaptive evolution is challenging to disentangle experimentally due to the complexity of mutation at the molecular level and difficulty of imposing directed selection in multicellular systems. In this way our work offers a framework that is complementary to ongoing experimental efforts to interrogate the evolution of GRNs and developmental patterning. Changes at the regulatory level is a fundamental avenue through which developmental patterns diversify[2–6]. Therefore, our findings and conceptual framework present a milestone towards a mechanistic understanding of the evolution of developmental patterns.

Whilst the dynamical mechanisms that can generate stripe-like patterns of gene expression are well established[47,69], much less is known about the evolutionary paths through which they emerge and diversify. Specifically, we lack a comprehensive understanding of feasible gene network modifications under selection for novel phenotypes, and how these changes are enabled or constrained by mutational processes and existing network architecture. By framing the evolution of the stripe phenotype as successively establishing and adjusting sharp gene expression boundaries, we identified the types of network modifications

commonly linked with specific phenotypic innovations. Our findings complement recent experimental work that has begun to investigate the relationship between mutation and pattern innovation[10]. Whilst a knowledge gap remains in linking molecular descriptions of genetic architecture to mechanistic models of GRN dynamics, deducing from the mechanistic requirements for a given patterning outcome possible molecular implementations, rather than vice versa, can explain "how the biological wood emerges from the molecular trees"[70] through evolutionary processes.

For example, we found a clear distinction between establishing gene expression boundaries *de novo* versus adjusting existing ones, with boundary adjustment typically occurring through smaller changes in the strength of gene interactions and new boundary establishment through larger changes. Smaller changes in transcription rates can be achieved through point mutations in binding sites or TF coding regions[37,71]. Larger changes could arise through duplication, resulting in multiple enhancers which then combine additively to control promoter activity[72]. We also found that the establishment of new boundaries typically required multiple new gene interactions to be introduced simultaneously, and an increase in the frequency of interaction sign changes. Novel interactions could arise through co-option[39], and whilst transcription factors are typically conserved as either inhibitors or activators, some can recruit multiple cofactors that have opposite effects depending on local sequence context[73]. Finally, whilst mutants could carry multiple simultaneous changes to GRN architecture – for example through mutation of a pleitropic TF coding region – we highlighted how neutral drift could also lead to the accumulation of multiple weight changes in the same individual. Our analysis therefore informs future experimental work by highlighting what type of network changes typically enable pattern innovation in an adaptive context, for which potential molecular mechanisms can then be proposed, engineered, and investigated experimentally.

An inherent property of GRN-mediated patterning is a degeneracy in network architecture, such that the genotype-to-phenotype map is characterised by a many-to-one relationship. Hence, multiple GRNs are able to generate the same spatial pattern[7,47,69]. Our repeated replays of *de novo* pattern evolution highlights the role of this degeneracy in the course of evolution, where we saw nearly identical phenotypic transitions in intermediate patterns. Variation instead emerged in GRN architecture, reflected in the topology and magnitude of

gene interactions. The way in which GRN architecture at a given time interacts with subsequent evolutionary processes is multi-faceted. For instance, existing architecture plays a critical role in determining which mutations confer a selective advantage. Functionally, this is because mutations typically affect components of the GRN that interact with pre-existing elements, thereby influencing the network's overall behaviour. Accordingly, the distribution of phenotypes generated in synthetic GRNs through random cis-regulatory mutations is specific to the GRN topology[9].

The dependence of phenotypic accessibility on GRN architecture alludes to historical contingency as an important aspect of GRN evolution, so that network changes accumulated early may influence subsequent evolution. We have built on this idea by investigating how the evolution of specific stripe forming mechanisms becomes contingent upon early network architecture. Using our predictive framework we identified "branching mutations" early in evolution which significantly altered the likely mechanistic outcome. This highlights that the constraints imposed by network architecture do not only refer to the patterning phenotypes that are accessible, but also the network changes which are feasible given specific selection pressures. This supports the idea that developmental bias – the differential accessibility of phenotypes induced by regulatory mechanism – should not be viewed as a static quantity, and itself has a phenotypic character[74] whose emergence can be contingent on historical mutations. In addition to identifying historical contingency as an important force in network evolution, we demonstrated how its emergence can be influenced through an interplay of selection and GRN architecture. For instance, at the first mutational step we identified a selective advantage associated with mutants carrying more weight changes, which manifested from the small target size of fit mutations and the sparse network connectivity. This was reflected in a higher realised mutation rate, and typically resulted in the accumulation of selectively-neutral weight changes. Interestingly, we demonstrated that these selectively neutral mutational changes often played an important role in biasing subsequent evolution towards a specific outcome, as has been demonstrated experimentally[68].

Future studies should aim to further develop modelling frameworks that integrate patterning mechanisms with mutation and selection in tandem with experimental work. For instance, synthetic biology offers a promising tool for testing evolutionary hypothesis[75],

and integrating synthetic tools with laboratory evolution could provide further mechanistic insight. Our high-throughput and tractable computational approach offers a conceptual framework to ground such future investigations. This dialogue between theory and experiment can ultimately distil how the molecular architecture that underlies GRN function governs evolutionary paths and constraints.

Acknowledgements We would like to thank Amy Bowen, James Briscoe, Jake Cornwall-Scoones, Leonard Dekens, James DiFrisco, Kabir Hussain, Taniya Mandal and Lewis Mosby for discussions and feedback on this work. This work was supported by the Francis Crick Institute, which receives its core funding from Cancer Research UK, the UK Medical Research Council, and Wellcome Trust.

References

1. Kicheva, A. & Briscoe, J. Control of Tissue Development by Morphogens. *Annu. Rev. Cell. Dev. Biol.* **39,** 91–121 (2023).
2. Méndez-González, I. D., Williams, T. M. & Rebeiz, M. Changes in locus wide repression underlie the evolution of Drosophila abdominal pigmentation. *PLOS Genet.* **19,** e1010722 (2023).
3. Sadier, A., Santana, S. E. & Sears, K. E. The Role of Core and Variable Gene Regulatory Network Modules in Tooth Development and Evolution. *Integr. Comp. Biol.* **63,** 162–175 (2023).
4. Johnson, M. R. *et al.* A multifunctional Wnt regulator underlies the evolution of rodent stripe patterns. *Nat. Ecol. Evol.* **7,** 2143–2159 (2023).
5. Onimaru, K., Marcon, L., Musy, M., Tanaka, M. & Sharpe, J. The fin-to-limb transition as the re-organization of a Turing pattern. *Nat. Commun.* **7,** 11582 (2016).
6. Prud'homme, B. *et al.* Repeated morphological evolution through cis-regulatory changes in a pleiotropic gene. *Nature* **440,** 1050–1053 (2006).
7. Santos-Moreno, J., Tasiudi, E., Kusumawardhani, H., Stelling, J. & Schaerli, Y. Robustness and innovation in synthetic genotype networks. *Nat. Commun.* **14,** 2454 (2023).
8. Baier, F., Gauye, F., Perez-Carrasco, R., Payne, J. L. & Schaerli, Y. Environment-dependent epistasis increases phenotypic diversity in gene regulatory networks. *Sci. Adv.* **9,** eadf1773 (2023).
9. Schaerli, Y. *et al.* Synthetic circuits reveal how mechanisms of gene regulatory networks constrain evolution. *Mol. Syst. Biol.* **14,** e8102 (2018).

10. Galupa, R. *et al.* Enhancer architecture and chromatin accessibility constrain phenotypic space during Drosophila development. *Dev. Cell* **58,** 51–62.e4 (2023).

11. Li, X. C. *et al.* Rapid response of fly populations to gene dosage across development and generations. *Nat. Commun.* **15,** 4551 (2024).

12. Sokolowski, T. R., Gregor, T., Bialek, W. & Tkačik, G. Deriving a genetic regulatory network from an optimization principle. *arXiv preprint arXiv:2302.05680* (2023).

13. Verd, B., Crombach, A. & Jaeger, J. Dynamic Maternal Gradients Control Timing and Shift-Rates for Drosophila Gap Gene Expression. *PLoS Comput. Biol.* **13,** e1005285 (2017).

14. Jaeger, J. *et al.* Dynamic control of positional information in the early Drosophila embryo. *Nature* **430,** 368–371 (2004).

15. Cohen, M. *et al.* Ptch1 and Gli regulate Shh signalling dynamics via multiple mechanisms. *Nat. Commun.* **6,** 6709 (2015).

16. Balaskas, N. *et al.* Gene Regulatory Logic for Reading the Sonic Hedgehog Signaling Gradient in the Vertebrate Neural Tube. *Cell* **148,** 273–284 (2012).

17. Pezzotta, A. & Briscoe, J. Optimal control of gene regulatory networks for morphogen-driven tissue patterning. *Cell Syst.* **14,** 940–952.e11 (2023).

18. Exelby, K. *et al.* Precision of tissue patterning is controlled by dynamical properties of gene regulatory networks. *Development* **148,** dev197566 (2021).

19. Verd, B., Monk, N. A. & Jaeger, J. Modularity, criticality, and evolvability of a developmental gene regulatory network. *eLife* **8** (eds Altenberg, L. & Wittkopp, P. J.) e42832 (2019).

20. Mousavi, R. & Lobo, D. Automatic design of gene regulatory mechanisms for spatial pattern formation. *NPJ. Syst. Biol. Appl.* **10,** 1–13 (2024).

21. Henry, A., Hemery, M. & François, P. Φ-evo: A program to evolve phenotypic models of biological networks. *PLoS Comput. Biol.* **14,** e1006244 (2018).

22. François, P. & Hakim, V. Design of genetic networks with specified functions by evolution in silico. *Proc. Natl. Acad. Sci.* **101,** 580–585 (2004).

23. Rothschild, J. B., Tsimiklis, P., Siggia, E. D. & François, P. Predicting Ancestral Segmentation Phenotypes from Drosophila to Anopheles Using In Silico Evolution. *PLOS Genet.* **12,** e1006052 (2016).

24. François, P., Hakim, V. & Siggia, E. D. Deriving structure from evolution: metazoan segmentation. *Mol. Syst. Biol.* **3,** 154 (2007).

25. Vroomans, R. M. A., Hogeweg, P. & ten Tusscher, K. H. W. J. In silico evo-devo: reconstructing stages in the evolution of animal segmentation. *EvoDevo* **7,** 14 (2016).

26. Fujimoto, K., Ishihara, S. & Kaneko, K. Network Evolution of Body Plans. *PLoS One* **3,** e2772 (2008).

27. Gould, S. J. *Wonderful Life: The Burgess Shale and the Nature of History* (WW Norton & Company, 1989).

28. Baker, C. R., Booth, L. N., Sorrells, T. R. & Johnson, A. D. Protein modularity, cooperative binding, and hybrid regulatory states underlie transcriptional network diversification. *Cell* **151,** 80–95 (2012).

29. Duncan, E. J., Benton, M. A. & Dearden, P. K. Canonical terminal patterning is an evolutionary novelty. *Dev. Biol.* **377,** 245–261 (2013).

30. Dalal, C. K. & Johnson, A. D. How transcription circuits explore alternative architectures while maintaining overall circuit output. *Genes Dev.* **31,** 1397–1405 (2017).

31. McQueen, E. & Rebeiz, M. On the individuality of gene regulatory networks: how does network re-use affect subsequent evolution? *Curr. Top. Dev. Biol.* **139,** 375–405 (2020).

32. Teichmann, S. A. & Babu, M. M. Gene regulatory network growth by duplication. *Nat. Genet.* **36,** 492–496 (2004).

33. Gutiérrez, J. & Maere, S. Modeling the evolution of molecular systems from a mechanistic perspective. *Trends Plant Sci.* **19,** 292–303 (2014).

34. Watson, J., Geard, N. & Wiles, J. Towards more biological mutation operators in gene regulation studies. *Biosystems* **76,** 239–248 (2004).

35. Friedlander, T., Mayo, A. E., Tlusty, T. & Alon, U. Mutation Rules and the Evolution of Sparseness and Modularity in Biological Systems. *PLoS One* **8,** e70444 (2013).

36. Stewart, A. J., Hannenhalli, S. & Plotkin, J. B. Why Transcription Factor Binding Sites Are Ten Nucleotides Long. *Genetics* **192,** 973–985 (2012).

37. Duque, T. & Sinha, S. What Does It Take to Evolve an Enhancer? A Simulation-Based Study of Factors Influencing the Emergence of Combinatorial Regulation. *Genome Biol. and Evol.* **7,** 1415–1431 (2015).

38. Jiménez-Delgado, S., Pascual-Anaya, J. & Garcia-Fernàndez, J. Implications of duplicated cis-regulatory elements in the evolution of metazoans: the DDI model or how simplicity begets novelty. *Brief. Funct. Genom.* **8,** 266–275 (2009).

39. Peter, I. S. & Davidson, E. H. Evolution of Gene Regulatory Networks Controlling Body Plan Development. *Cell* **144,** 970–985 (2011).

40. Majic, P. & Payne, J. L. Enhancers Facilitate the Birth of De Novo Genes and Gene Integration into Regulatory Networks. *Mol. Biol. Evol.* **37,** 1165–1178 (2020).

41. Igler, C., Lagator, M., Tkačik, G., Bollback, J. P. & Guet, C. C. Evolutionary potential of transcription factors for gene regulatory rewiring. *Nat. Ecol. Evol.* **2,** 1633–1643 (2018).

42. Khatri, B. S., McLeish, T. C. B. & Sear, R. P. Statistical mechanics of convergent evolution in spatial patterning. *Proc. Natl. Acad. Sci.* **106,** 9564–9569 (2009).

43. Greenbury, S. F., Louis, A. A. & Ahnert, S. E. The structure of genotype-phenotype maps makes fitness landscapes navigable. *Nat. Ecol. Evol.* **6,** 1742–1752 (2022).

44. Kimura, M. On the Probability of Fixation of Mutant Genes in a Population. *Genetics* **47,** 713 (1962).

45. Proulx-Giraldeau, F., Rademaker, T. J. & François, P. Untangling the Hairball: Fitness-Based Asymptotic Reduction of Biological Networks. *Biophys. J* **113,** 1893–1906 (2017).

46. Burda, Z., Krzywicki, A., Martin, O. C. & Zagorski, M. Motifs emerge from function in model gene regulatory networks. *Proc. Natl. Acad. Sci.* **108,** 17263–17268 (2011).

47. Cotterell, J. & Sharpe, J. An atlas of gene regulatory networks reveals multiple three-gene mechanisms for interpreting morphogen gradients. *Mol. Syst. Biol.* **6,** 425 (2010).

48. Clyde, D. E. *et al.* A self-organizing system of repressor gradients establishes segmental complexity in Drosophila. *Nature* **426,** 849–853 (2003).

49. Mangan, S. & Alon, U. Structure and function of the feed-forward loop network motif. *Proc. Natl. Acad. Sci.* **100,** 11980–11985 (2003).

50. Shi, W., Ma, W., Xiong, L., Zhang, M. & Tang, C. Adaptation with transcriptional regulation. *Sci. Rep.* **7,** 42648 (2017).

51. Uygur, A. *et al.* Scaling Pattern to Variations in Size during Development of the Vertebrate Neural Tube. *Dev. Cell* **37,** 127–135 (2016).

52. Hinman, V. F., Nguyen, A. T., Cameron, R. A. & Davidson, E. H. Developmental gene regulatory network architecture across 500 million years of echinoderm evolution. *Proc. Natl. Acad. Sci.* **100,** 13356–13361 (2003).

53. Kogenaru, M., Nghe, P., Poelwijk, F. J. & Tans, S. J. Predicting Evolutionary Constraints by Identifying Conflicting Demands in Regulatory Networks. *Cell Syst.* **10,** 526–534.e3 (2020).

54. Jiménez, A., Cotterell, J., Munteanu, A. & Sharpe, J. Dynamics of gene circuits shapes evolvability. *Proc. Natl. Acad. Sci.* **112,** 2103–2108 (2015).

55. Gitschlag, B. L., Cano, A. V., Payne, J. L., McCandlish, D. M. & Stoltzfus, A. Mutation and Selection Induce Correlations between Selection Coefficients and Mutation Rates. *Am. Nat.* **202,** 534–557 (2023).

56. Reeves, G. T. The engineering principles of combining a transcriptional incoherent feedforward loop with negative feedback. *J. Biol. Eng.* **13,** 62 (2019).

57. Whitehead, D. J., Wilke, C. O., Vernazobres, D. & Bornberg-Bauer, E. The look-ahead effect of phenotypic mutations. *Biol. Direct* **3,** 18 (2008).

58. Lynch, M. Mutation pressure, drift, and the pace of molecular coevolution. *Proc. Natl. Acad. Sci.* **120,** e2306741120 (2023).

59. Nghe, P. *et al.* Predicting Evolution Using Regulatory Architecture. *Annu. Rev. Biophys.* **49,** 181–197 (2020).

60. Husain, K. & Murugan, A. Physical Constraints on Epistasis. *Mol. Biol. Evol.* **37,** 2865–2874 (2020).

61. Tyler, A. L., Asselbergs, F. W., Williams, S. M. & Moore, J. H. Shadows of complexity: what biological networks reveal about epistasis and pleiotropy. *Bioessays* **31,** 220–227 (2009).

62. Wong, T. Y. W. Sources of evolutionary contingency: chance variation and genetic drift. *Biol. Philos.* **35,** 36 (2020).

63. Ijäs, T. & Koskinen, R. Exploring biological possibility through synthetic biology. *Euro. Jnl. Phil. Sci.* **11,** 39 (2021).

64. DiFrisco, J. & Wagner, G. P. Body Plan Identity: A Mechanistic Model. *Evol. Biol.* **49,** 123–141 (2022).

65. Barton, N. H. Genetic hitchhiking. *Philos. Trans. R. Soc. Lond. B. Biol. Sci.* **355,** 1553–1562 (2000).

66. Zheng, J., Payne, J. L. & Wagner, A. Cryptic genetic variation accelerates evolution by opening access to diverse adaptive peaks. *Science* **365,** 347–353 (2019).

67. Lundberg, S. M. & Lee, S.-I. *A Unified Approach to Interpreting Model Predictions* in *Adv. Neural Inf. Process. Syst.* **30** (Curran Associates, Inc., 2017).

68. Sorrells, T. R., Booth, L. N., Tuch, B. B. & Johnson, A. D. Intersecting transcription networks constrain gene regulatory evolution. *Nature* **523,** 361–365 (2015).

69. Schaerli, Y. *et al.* A unified design space of synthetic stripe-forming networks. *Nat. Commun.* **5,** 4905 (2014).

70. Gunawardena, J. Models in biology: 'accurate descriptions of our pathetic thinking'. *BMC Biol.* **12,** 29 (2014).

71. Lässig, M. From biophysics to evolutionary genetics: statistical aspects of gene regulation. *BMC Bioinformatics* **8,** S7 (2007).

72. Martinez-Ara, M., Comoglio, F. & van Steensel, B. Large-scale analysis of the integration of enhancer-enhancer signals by promoters. *eLife* **12** (2024).

73. Rosenfeld, M. G., Lunyak, V. V. & Glass, C. K. Sensors and signals: a coactivator/-corepressor/epigenetic code for integrating signal-dependent programs of transcriptional response. *Genes Dev* **20,** 1405–1428 (2006).

74. Uller, T., Moczek, A. P., Watson, R. A., Brakefield, P. M. & Laland, K. N. Developmental Bias and Evolution: A Regulatory Network Perspective. *Genetics* **209,** 949–966 (2018).

75. Baier, F. & Schaerli, Y. *Addressing Evolutionary Questions with Synthetic Biology* in *Evolutionary Systems Biology: Advances, Questions, and Opportunities* (ed Crombach, A.) 135–157 (Springer International Publishing, Cham, 2021).

76. McInnes, L., Healy, J., Saul, N. & Großberger, L. UMAP: Uniform Manifold Approximation and Projection. *J. Open Source Softw.* **3,** 861 (2018).

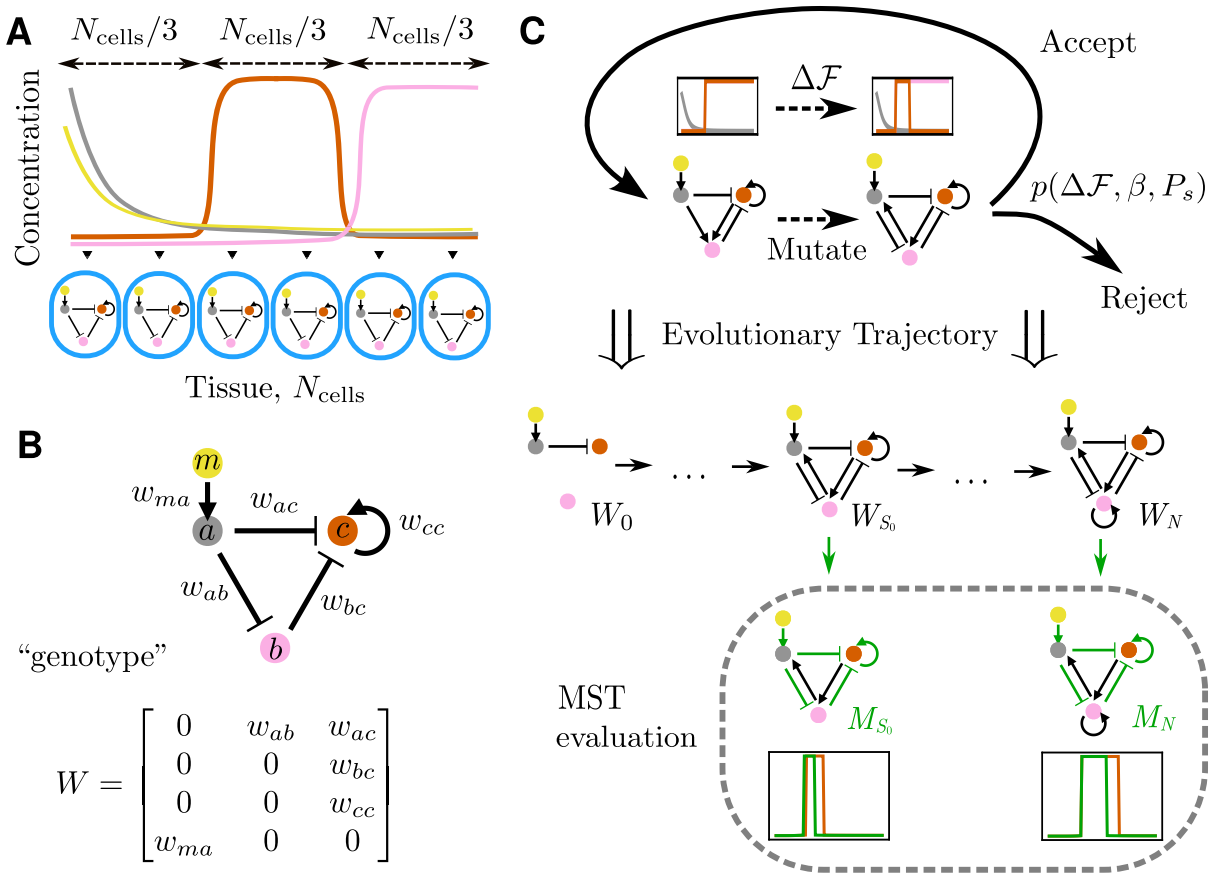

Figure 1: **Method Summary** A. Model of developmental patterning and target stripe. A tissue is made up of a discrete number of cells (blue ovals), each with an identical 3-node gene regulatory network (GRN). A morphogen gradient (yellow) is assumed to be at steady state across the tissue. The target stripe profile (orange) has boundaries which define three equal size regions across the tissue. B. An example GRN. The morphogen, m (yellow) activates gene a (grey), which then regulates the output gene c (orange) directly and through an intermediary gene b (pink). The regulatory organisation is specified by a matrix W that holds the weights that define an effective strength for activation (positive weights) and inhibition (negative weights) arrows, and represents the genotype in our analysis. C. A schematic outlining the Monte-Carlo scheme for simulating evolutionary trajectories. The resident genotype associated with the current phenotype is mutated by introducing or editing existing interactions (weight changes). The new phenotype defines a fitness differential $\Delta\mathcal{F}$, which then determines the probability $p(\Delta\mathcal{F}, \beta, P_s)$ of fixation for the mutant based on the selection strength β and population size P_s. This process then repeats until a predefined fitness threshold is reached. The sequence of accepted mutants is collected to form an "evolutionary trajectory". The MST (*minimal stripe topology*) associated with the first stripe forming mutant W_{S_0} and the final mutant W_N are then evaluated. The MST is the topology associated with the minimal set of regulatory interactions able to maintain a stripe phenotype. Details of parameters used in the evolutionary algorithm are provided in SM.

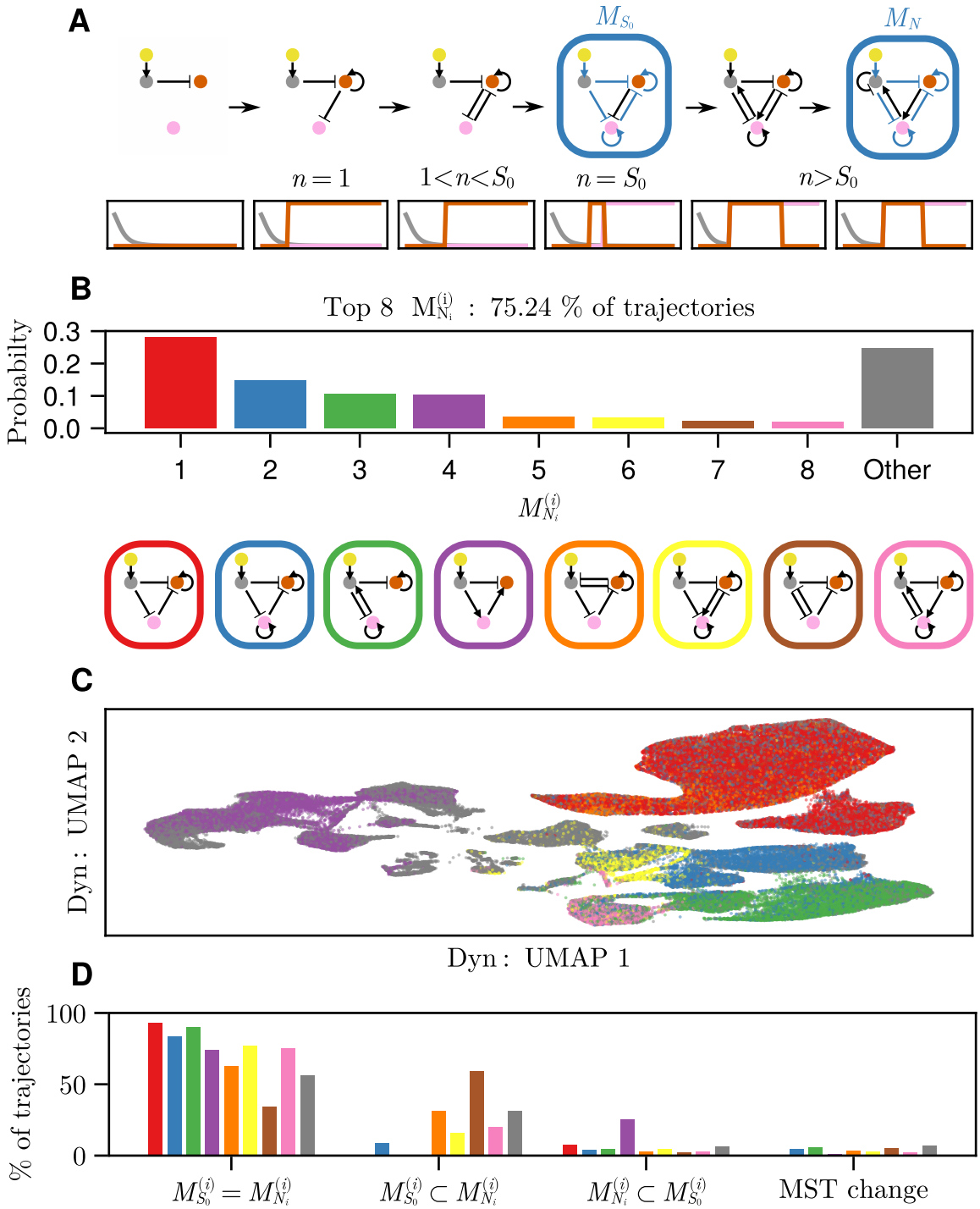

Figure 2: **The distribution of adaptive outcomes relating to the core mechanisms of stripe formation.** A. An example evolutionary trajectory showing topological changes in the underlying network along with the associated phenotypes. Each step indicates an accepted mutant. The change in the network topology (genotype) is shown on top with the corresponding gene expression profile (phenotype) below. The value of n is the index of the shown accepted mutant. The interactions which form the MST at $n = S_0$ and $n = N$ are highlighted and denoted as M_{S_0} and M_N respectively. B. The distribution of final MST outcomes $M_{N_i}^{(i)}$ across evolutionary simulations. Colours correspond to the MSTs visualized below the distribution. The "other" category corresponds to 724 additional MSTs, and hence represents the tail of the outcome distribution. C. A UMAP[76] embedding of the dynamics associated with final evolved networks $W_{N_i}^{(i)}$, with colour coding indicating MST classification shown in B. D. The proportion of trajectories pertaining to the four different cases describing the relation of the first stripe-forming MST and the final MST, split by final MST outcome. The four cases are: MST preservation ($M_{S_0}^{(i)} = M_{N_i}^{(i)}$), complexification ($M_{S_0}^{(i)} \subset M_{N_i}^{(i)}$), simplification ($M_{N_i}^{(i)} \subset M_{S_0}^{(i)}$) and MST change ($M_{S_0}^{(i)} \not\subset M_{N_i}^{(i)} \wedge M_{N_i}^{(i)} \not\subset M_{S_0}^{(i)}$).

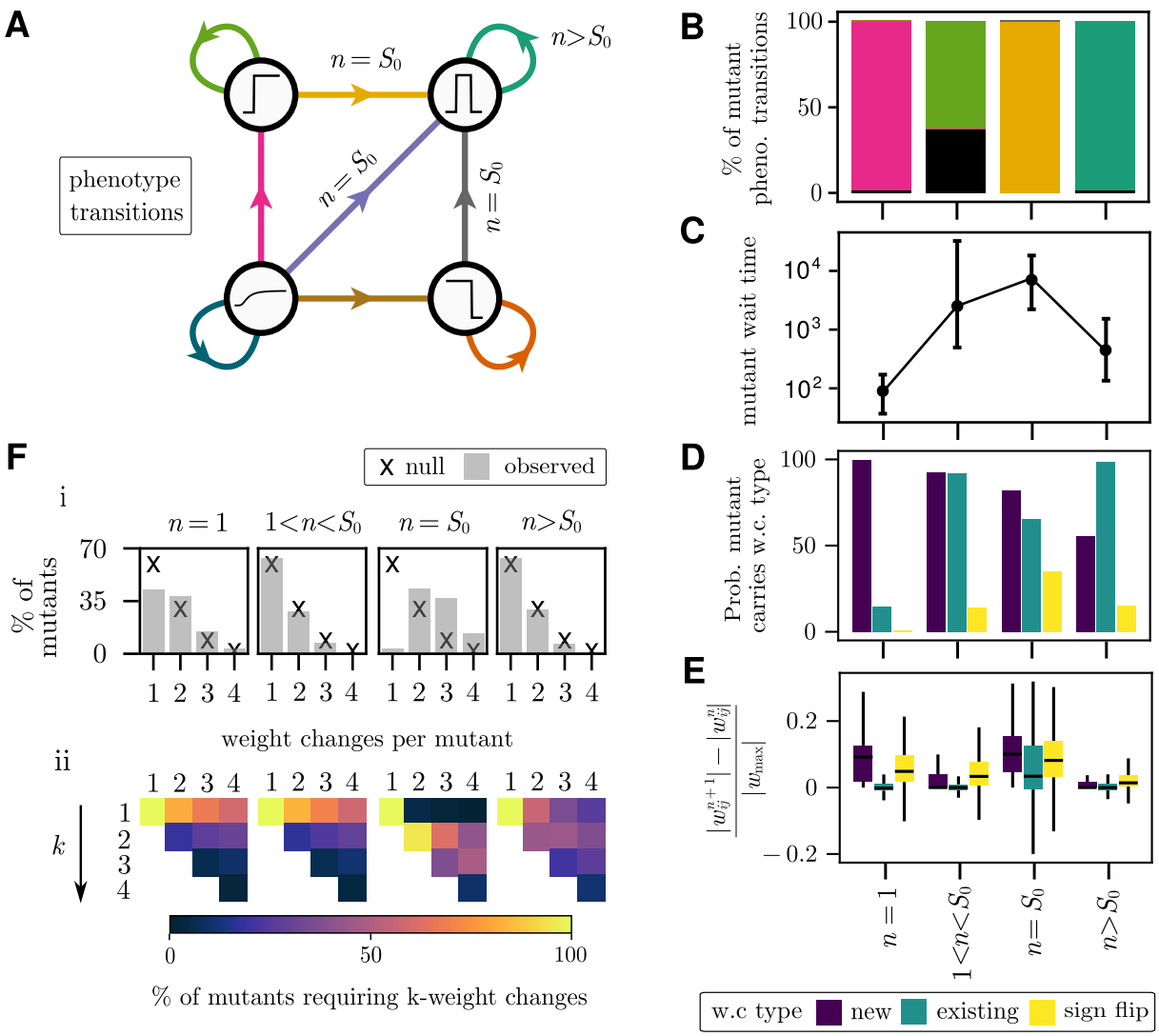

Figure 3: **Key components of stripe evolution.** A. Phenotypic transitions during evolution. The initial phenotype is that of a shallow left-boundary (bottom left). The first accepted mutant at $n = 1$ may lead to a sharp left boundary (top left, pink arrow), a stripe (top right, purple arrow), a sharp right boundary (bottom right, brown arrow) or adjust the existing phenotype without introducing new boundaries (self arrow). Arrows between these states indicate the acceptance of a mutant driving the respective phenotypic changes. Self-arrows indicate accepted mutants that adjust the respective phenotype without adding or removing boundaries. Arrows for transitions that lead to stripe inception are marked by $n = S_0$. B. Percentage of accepted mutants in different evolutionary periods associated with specific phenotype transitions. Colours correspond to arrows in A. The black bar for $1 < n < S_0$ corresponds to neutral mutants that do not induce a phenotypic shift or fitness change. C. Median wait times associated with accepted mutants in each evolutionary period (dots). Range bars represent the 25th to 75th percentiles of the wait time distribution. D. Classification of the weight change (w.c.) types carried by accepted mutants in different evolutionary periods as follows: introduction of a new weight (purple), adjustment of existing weight while preserving sign (green) adjustment of existing weight with sign change (yellow). Solid bars indicate the probability of mutants carrying at least one weight change of the type corresponding to the colour. E. The distribution of weight change magnitudes expressed relative to the maximum regulatory effect, defined as $|w_{ij}^{n+1}| - |w_{ij}^{n}|/|w_{\max}|$, associated with mutants in different evolutionary periods. Colour indicates weight change category as in D. F. Percentage of accepted mutants carrying 1-4 weight changes, across different evolutionary periods. Crosses indicate likelihood according to null sampling distribution (pre-selection), bars indicate post selection percentages. For each mutant carrying multiple weight changes we evaluate the minimum number of weight changes, k, required to produce the observed fitness gain. This information is visualized in the heatmap, which presents the distribution of required weight changes k against the original number carried by the mutants. Yellow along diagonal entries indicates that all weight changes are necessary for the fitness gain.

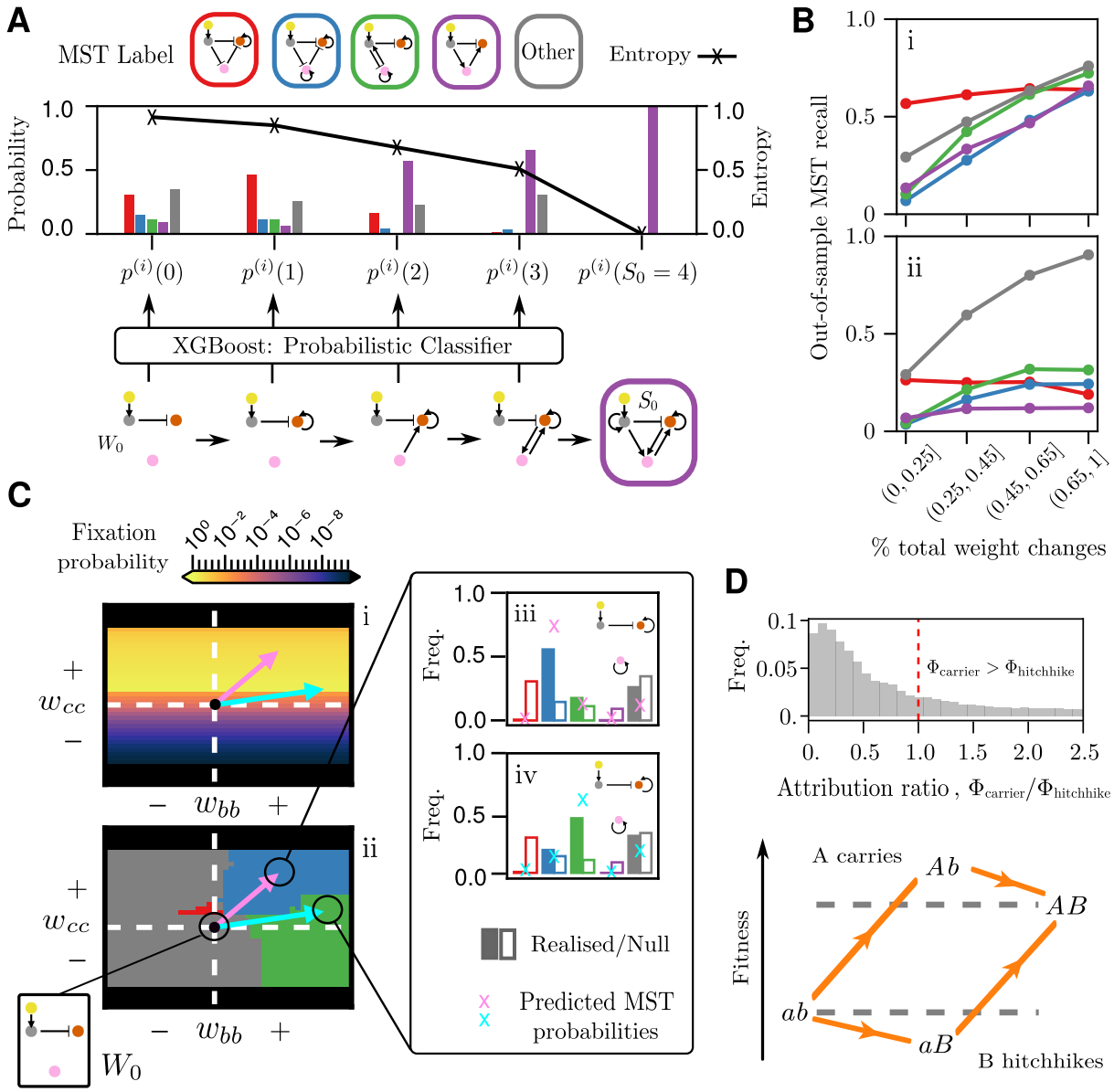

Figure 4: **Predictability of stripe evolution.** A. An example trajectory and the MST prediction probabilities for intermediate mutants. Colours (Red,Blue,Green and Purple) represent MST labels and correspond to colour coding used in Figure 2, with grey representing the "other" MST category. A sequence of network configurations corresponding to fixed mutants in an example trajectory i is shown, with the MST realised at S_0 shown highlighted in purple, corresponding to MST:4. For each network $W_k^{(i)}$ in the $i-$th trajectory we produce a probabilistic MST prediction $p^{(i)}(k)$ using a trained XGBoost classifier. Here $p^{(i)}(k) = [p_1^{(i)}(k), p_2^{(i)}(k), p_3^{(i)}(k), p_4^{(i)}(k), p_{\text{other}}^{(i)}(k)]$ where $p_j^{(i)}(k)$ is the probability that the j-th MST is realised at S_0 given the k-th mutant. Coloured bars indicate the individual MST prediction probabilities $p_j^{(i)}$. Black line indicates entropy associated with the prediction probabilities $p^{(i)}(k)$. B. The recall for each MST outcome evaluated on out-of sample networks at different stages of evolution, evaluated using the complete predictive model (i) and the topology only predictive model (ii). Networks were first binned according to the number of weight edits they had accumulated as a percentage of the total accumulated at S_0. The bins were chosen so that the number of networks in each bin across the sample was approximately equal. Next, the recall for each MST outcome was evaluated for the networks in each bin. Recall is the % of correct predictions for the outcome. A prediction is deemed correct if it matches the MST outcome and furthermore, persists from the point of prediction to S_0 - for more details see SM. C. 2-dimensional fitness landscapes associated with pairwise weight changes carried by the ($n = 1$) mutant (i) with the associated MST predictions (ii). Pink and cyan arrows indicate weight changes associated with selected branching mutations. Bar charts (iii) and (iv) represent the MST outcome distributions associated with pink and cyan branching mutations. Filled bars indicate the distribution induced by the branching mutations, whereas non-filled bars represent the null distribution ($\mathbb{P}(M_{S_0}^{(i)} = j|W_0)$). Scatter crosses indicate probability of each MST outcome given by predictive model for the branching mutants. D. Histogram showing the distribution of prediction attribution ratios $\Phi_{\text{carrier}}/\Phi_{\text{carrier}}$ associated with mutants carrying hitchhiking weight changes. Red dashed line indicates equal attribution between hitchhiking and carrier weight changes, with left and right regions indicating greater attribution associated with hitchhiking or carrier weight changes respectively.